THE UNIVERSITY OF WARWICK

Original citation:
Dang, Hiep Vu and Živanović, Stana. (2015) Experimental characterisation of walking locomotion on rigid level surfaces using motion capture system. Engineering Structures, Volume 91 . pp. 141-154.

Permanent WRAP url:
http://wrap.warwick.ac.uk/69564

A note on versions:
The version presented here may differ from the published version or, version of record, if you wish to cite this item you are advised to consult the publisher's version. Please see the 'permanent WRAP url' above for details on accessing the published version and note that access may require a subscription.

For more information, please contact the WRAP Team at: publications@warwick.ac.uk

warwickpublicationswrap

highlight your research

http://wrap.warwick.ac.uk

Experimental characterisation of walking locomotion on rigid level surfaces using motion capture system

HIEP VU DANG
STANA ŽIVANOVIĆ

Address of the corresponding author:

Dr Stana Živanović
Associate Professor
University of Warwick
School of Engineering
Coventry CV4 7AL
United Kingdom

E-Mail: s.zivanovic@warwick.ac.uk

Phone: +44 (0) 24 765 28392

Fax: +44 (0) 24 764 18922

ABSTRACT

Low-frequency structures, such as footbridges and long-span floors, are often sensitive to variations in dynamic loading induced by pedestrians. As a result, the design of these structures using traditional deterministic approaches is being replaced by stochastic load models that can accommodate different styles of walking. To inform development and facilitate wider implementation of the new stochastic approaches, a database of experimental data characterising both inter- and intra-subject variability of gait parameters is required. This study aims to contribute to the development of such a database by providing a set of data for walking over rigid level surfaces.

The motion capture system Vicon was used for simultaneous monitoring of the kinematic and kinetic gait parameters. Ten test subjects walking at 13 different speeds participated in the experimental programme. Novel experimental data on pacing rate, step length, step width, angular positions of the legs and the trunk, and the force amplitude were collected and statistically characterised. The acquired data are suitable for calibration of the bipedal pedestrian models intended for civil engineering applications.

Keywords: Walking locomotion, Inter-subject and intra-subject variability, Motion capture system, Force reconstruction.

1   Introduction

Reliable assessment of vibration serviceability of low-frequency civil engineering structures exposed to pedestrian excitation, such as footbridges and long-span floors, requires the development of sophisticated models of walking locomotion. Deterministic models based on ''average pedestrian'' properties [1] are not always suited for the design of contemporary structures since these, typically light, slender and lightly damped, structures are increasingly sensitive to variations in dynamic excitation. To account for these variations, stochastic modelling approaches could be utilised. Significant advances in the development of the stochastic models have been made over the last decade [2–7]. All these models aim to mathematically describe the force waveform generated when walking on rigid level surfaces. The models range from a simple incorporation of randomness in the pacing frequency within a human population (e.g. [3]) to those that replicate the intrinsic narrow-band nature of the dynamic force induced by a single individual (e.g. [5]). The stochastic models are most often informed by empirical data related to the following walking locomotion parameters: walking speed, force amplitude, pacing rate, step length and step width.

Increased liveliness of modern structures carrying pedestrian traffic poses a new challenge to structural engineers due to a need to model a pedestrian as a part of a pedestrian-structure vibrating system. Within this system, the pedestrian is exposed to the structural acceleration that might modify their walking locomotion style and consequently alter both the temporal and spectral features of the structural vibration [8]. Modelling the walking locomotion in this case is a challenge since it requires a departure from replicating the force waveform measured on a rigid surface. The challenge can be addressed, for example, by modelling the force profile measured on a lively (i.e. oscillating) surface or by developing fundamental models of pedestrians and their interaction with oscillating supporting structure. The former approach requires the development of an experimental setup that allows for measuring the walking-induced force at a range of vibration frequencies and vibration amplitudes. The latter approach

intends to represent the source of the dynamic force, i.e. mechanics of walking locomotion, accurately. Inclusion of the locomotor system (i.e. legs) into the modelling introduces a capability to account for kinematic conditions at the human foot – structure interface, making these models potentially suitable for representing walking over both rigid and vibrating surfaces. Biomechanically inspired bipedal pedestrian models belong to this class and they are already being developed for civil engineering applications [9,10]. To successfully calibrate these models, experimental data are required not only on the walking speed, force amplitude, pacing rate, step length and step width, but also on angular positions of the legs. Ideally the data should include information about both the variability of walking locomotion parameters in a population of different individuals (so called inter-subject variability) and the intrinsic variations in the locomotion parameters induced by a single individual on a step-by-step basis (so called intra-subject variability). It is the intention of this study to provide the experimental data that could be used for calibration of bipedal models.

Data about a wide range of walking locomotion parameters are available in literature in different forms and with different levels of detail. They are, however, rarely acquired simultaneously due to limitations in measurement techniques employed. For example, frequently used force plate and instrumented treadmill devices cannot measure the angular position of the legs. In addition, the collection of a set of data is often performed with a specific application in mind (such as medical rehabilitation) leading to measuring a small subset of parameters that are most relevant for the particular application and presentation of results in a form that is not necessarily suitable for the development of pedestrian models in civil engineering.

When the walking speed, step length, step width, pacing rate and force amplitude for a pedestrian are measured, an average value for each parameter is usually reported. To characterise the inter-subject variability, the mean and the coefficient of variation (CoV) of the average value within a studied population are then calculated. Several examples of the mean

and CoV for the (average) parameters reported in literature are: 1.87 Hz and 10% for the pacing frequency, 1.39 m/s and 14% for the walking speed, 0.74 m and 11% for the step length [11], and 95 mm and 19% for the step width [12]. Three among these parameters (walking speed v, step length d and pacing frequency f_p) are mutually dependent ($v = d\,f_p$) and therefore defining any two will automatically determine the third. To model all these parameters, a normal distribution is frequently employed [13]. As for the dynamic force, it is most often reported in the form of the dynamic loading factors DLF_i (i = 1–4) which represent the amplitude of the i-th main forcing harmonic normalised by the pedestrian weight. Kerr [14] found that the mean value of first main harmonic (DLF_1) increases with an increase in the pacing frequency up to 2.2Hz. Beyond 2.2 Hz, the amplitude remains fairly constant. He also reported that the CoV for this parameter is about 16%. Furthermore, Geyer [15] showed that the attack angle tends to decrease linearly from 75° to 67° with an increase in the walking speed from 0.6 m/s to 2.4 m/s while the end-of-step angle is rarely quantified. Definition of the two angular parameters differs slightly between studies, depending on the experimental setup used to monitor the kinematics of the test subject's body. In the context of this study the attack angle is defined as the angle between the line connecting body's centre of mass (BCoM) and the foot of the leading leg (at the heel-strike event) and the walking surface. The end-of-step angle is taken as the angle formed by the line connecting BCoM and the foot of the trailing leg (at the toe-off event) and the walking surface. Some studies also report the trunk rotation over an individual step. Although this rotation is small at about 2°, it still can make a significant contribution to some walking locomotion quantifiers, such as the moment about the hip joint [16].

The average value of a parameter for an individual pedestrian provides no insight into the intra-subject variability. For this, the variation in pedestrian parameters (i.e. their CoV) on a step-by-step basis has to be known. Within an investigated pedestrian population this variation can be expressed using the mean and the standard deviation of the CoV. Information of this type is often scarce and incomplete. For example, Brownjohn et al. [2] provided useful information

that the CoV of pacing frequency on a step-bystep basis is around 3%, while Bauby and Kuo [17] found that the variability in the step width is larger than in the step length. In both cases, however, additional information about a potential correlation of the investigated parameters with, for example, the pacing frequency or the walking speed was not studied. Yamasaki et al. [18], on the other hand, provided detailed information on the variations in the step length. They found that the mean CoV ranges from 2% to 5% and that it is a function of the walking speed and gender. They also provided data for the standard deviation for both genders and a range of speeds. This study represents an example of a detailed description of the intra-subject variability (and its variation across a population of test participants) that can be used as a direct input into stochastic modelling.

To monitor key parameters of interest (i.e. walking speed, pacing rate, step length, step width, DLF, attack angle, end-of-step angle, and trunk rotation) simultaneously, a motion capture system (MCS) that tracks human body movement can be employed. Use of the MCS only is straight forward for measuring all parameters except the DLF which, in this case, has to be evaluated indirectly from the measured kinematic data. Using the MCS for measuring human-induced force while jumping, bouncing, running and walking is relatively new (and still rare) in civil engineering applications [19–21]. This is the most likely reason behind the lack of guidance on both the best tracking model that should be employed in these experiments and the accuracy that can be achieved.

The main aim of this paper is to statistically characterise the walking locomotion parameters on a population of ten test subjects. Particular attention is devoted to characterising the intra-subject variability and testing the hypothesis of whether the step-by-step variations in the parameters follow a normal distribution. The study also aims to provide some insight into the choice of the MCS-based tracking models for indirect measurements of the dynamic force. To achieve these aims, an experimental study of human walking locomotion on a rigid surface was conducted. The data collected are expected to find use in the process of calibration of the

bipedal class of pedestrian models. The natural next step would be to validate these models against the walking locomotion parameters acquired in the presence of the pedestrian-structure interaction; a task that is beyond the scope of this paper. Since the bipedal models are most likely to be used on structures prone to the excitation by the first forcing harmonic, only DLF_1 is considered in this study. This research is exclusively concentrated on the vertical component of the force.

Following this introductory section, an investigation into the use of the MCS for measuring human-induced dynamic force is presented. Apart from the background information on the indirect force measurements, the MCS employed in this study is described and an analysis related to the choice of a tracking model is performed. The main experimental investigation into the variability of walking locomotion parameters is then presented. Finally, a statistical characterisation of the parameters in a form suitable for future use is conducted, followed by a discussion and conclusions.

All experiments reported in this paper were approved by the Biomedical and Scientific Research Ethics Committee at the University of Warwick. Prior to the experiments, the test procedure and associated health and safety issues were explained to the test subjects (TSs). In addition, TSs signed a consent form and completed a physical readiness questionnaire. Only TSs with no health issues at the time of testing were allowed to take part in the experiments.

2   Measuring dynamic force using motion capture system

A MCS consists of a series of video-based optoelectronic cameras or sensors that are used to capture displacement of markers attached to human anatomical landmarks. Kinematic data of body segments recorded in this way have been used to reconstruct the human-induced force during walking [19], bouncing and jumping [20] and running [21].

According to Newton's second law, the vertical component of the force $F_z(t)$ generated by a pedestrian is:

$$F_z(t) = \underbrace{m_p \ddot{z}_{BCoM}}_{F_D(t)} + \underbrace{m_p g}_{W} \tag{1}$$

where F_D and W are the dynamic and static components of the walking-induced force, respectively, m_p is the body mass, $\ddot{z}_{BCoM}$ is the vertical acceleration of the BCoM caused by walking (positive upwards), and g = 9.81 m/s^2. In the walking posture, the BCoM is normally located inside the human body, and therefore its acceleration cannot be directly measured. Instead, the segmental method for estimating the acceleration, and therefore the force, is frequently used [21,22]. The method assumes that the human body consists of a chain of rigid segments: head, upper arms, forearms, hands, trunk, thighs, shanks and feet. The total force is calculated by summing the contributions from the individual segments:

$$F_z(t) = \sum_{i=1}^{k} m_i(\ddot{z}_i + g) \tag{2}$$

where m_i is the mass of the i-th body segment, $\ddot{z}_i$ is the vertical acceleration of the corresponding segment's centre of mass (SCoM), while k is the number of segments. The use of this equation relies on estimating body segment parameters (i.e. the segment mass and the position of the SCoM) from the databases available. A comprehensive database for a sample of 100 male test subjects was developed by de Leva in 1996 [23], and it is summarised in Table 1. The mass of each body segment is expressed as a percentage of the body mass, while the location of each SCoM is defined as a percentage of the segment length measured from the top end for the trunk segment and from the proximal end-point (i.e. the end point closer to the trunk) for other body segments. Examples of three body segments are shown in Fig. 1, while detailed description of all segments is available in [23]. The data in Table 1 allow representation of the trunk as either a single body segment having mass of 43.5% or three body segments having individual masses of 16.0%, 16.3% and 11.2%.

The assumption that the body segments are rigid is not strictly correct. Namely, the deformability of the soft tissue relative to the underlying bones induces errors in the measured

kinematic data [22]. This error, known as the soft tissue artefact, is most prominent at those stages of walking characterised by high accelerations, such as heel impacts. The problem mainly affects the high frequency content of the measured signals, and it can usually be minimised by low-pass filtering of the raw kinematic data [22].

In civil engineering applications, the segmental method has been successfully used by Racic et al. [20] to quantify bouncing and jumping forces, while the potential to use the same method for measuring the vertical component of the walking-induced forces has been demonstrated by the same authors on a single test subject only [19]. To utilise the method in this study, it is necessary to identify a marker layout to be employed in the experimental programme. The literature does not provide either guidance on the choice of the marker model or advice on the accuracy that can be achieved. For this reason four candidate marker models are investigated in more detail in this section.

Table 1
Average body segment parameters for a population of 100 male test subjects [23].

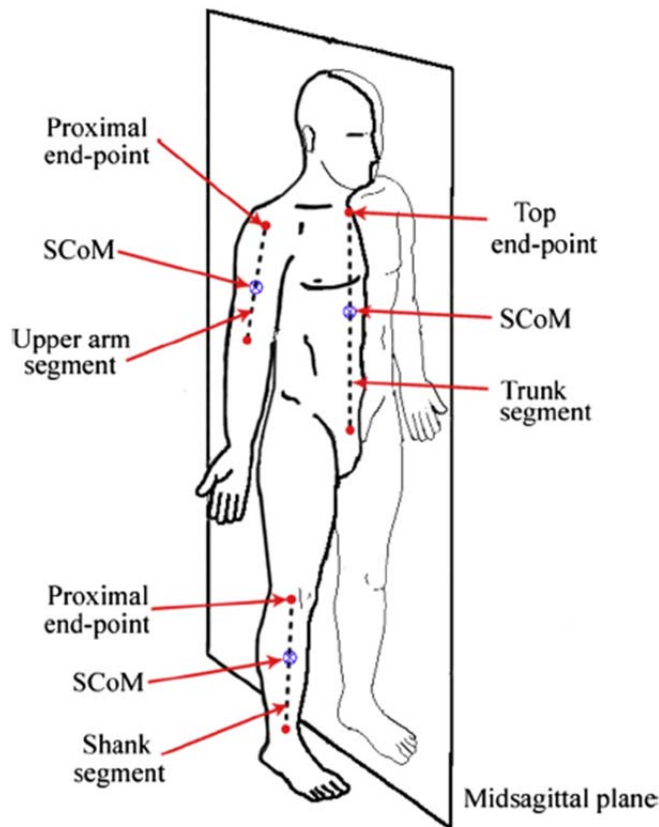| Body segment	Mass (%)	SCoM (%)
Head	6.9	40.2
Trunk	43.5	44.9
Upper arm	2.7	57.7
Forearm	1.6	45.7
Hand	0.6	79.0
Thigh	14.2	41.0
Shank	4.3	44.6
Foot	1.4	44.2
Upper trunk	16.0	30.0
Middle trunk	16.3	45.0
Lower trunk	11.2	61.2
Population properties:	Age: 23.8 (6.2) (year)	
mean (standard deviation) (unit)	Height: 174.1 (6.2) (cm)	
	Mass: 73.0 (9.1) (kg)	

Figure 1: Three body segments and the midsagittal plane (adapted from [24]).

2.1 Measurement system

Experiments for testing the performance of the marker models were performed in the Gait Laboratory, equipped with a motion capture system Vicon [25] and a force plate OR6-7-2000 [26], at the University of Warwick.

The MCS consists of twelve high-speed and low latency cameras that record 200 two-dimensional frames per second. Fig. 2a shows the layout of the cameras covering a capture volume of 2.0 x 3.0 x 2.2 m(width x length x height). The spherical markers, coated with a highly retro-reflective material, have a diameter of 14 mm and a mass of 2g. The front of each camera contains a strobe unit configured with light-emitting diodes to illuminate the markers. When a marker is inside the field of view of a specific camera, rays of light from the strobe unit illuminate the marker and are reflected back to the camera lens. The image from each camera is then processed by the system resulting in a reconstruction of displacement trajectories of the

markers in the three-dimensional space. For successful reconstruction, each marker has to be tracked simultaneously by at least two cameras.

Before starting the measurements, the relative distances between cameras and their projections were established by waving a calibration wand of a known geometry (Fig. 2b) inside the capture volume. The wand was also used to set the origin of the global coordinate system (Fig. 2b). The background noise was determined by monitoring stationary markers for 30 s [27]. The one second root-mean-square value of the measured noise was found to be less than 0.05 mm, which is an acceptable noise level for the current study.

The force plate (of size 464 x 508 mm) in the Gait Laboratory is mechanically isolated from the surrounding floor (Fig. 2b). The fundamental natural frequency of the plate in the vertical direction is 530 Hz, which is well above the frequency content in the force signal studied, making the force plate suitable for the intended experiments.

Recordings of the marker trajectories and the force plate signal were synchronised using an MX Giganet data acquisition unit [25], making direct comparisons of the time domain events in the two signals possible.
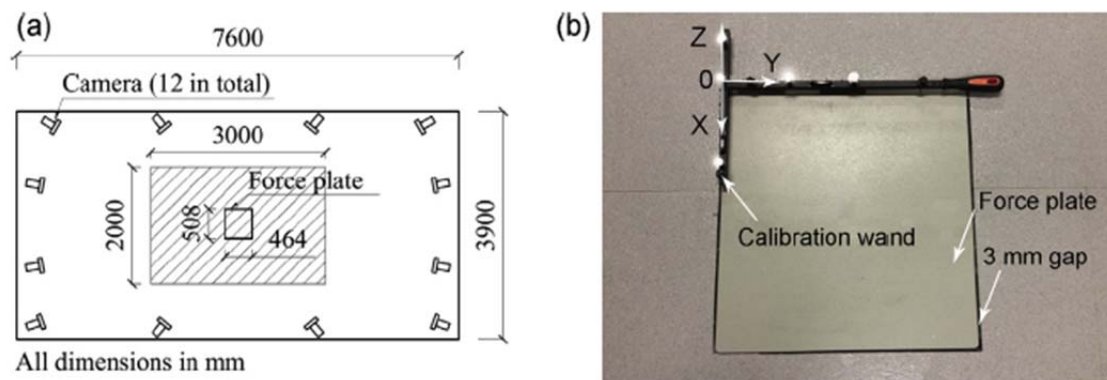

Figure 2: (a) Plan layout of the Gait Laboratory. (b) Force plate and calibration wand.

2.2 Marker models

Each test subject was instrumented using 34 markers (Fig. 3). Fifteen markers were positioned on either half of the body, while the remaining four markers (No. 9, 10, 11 and 14 in Fig. 3) were located in the midsagittal plane (Fig. 1). The marker positions were chosen to provide data on kinematics of individual body segments, and they were informed by the literature related to the research in: balance during standing, modelling BCoM's trajectory and the force reconstruction for different human activities. Four marker models (Models A, B, C and D) were formulated (Fig. 3). The exact anatomical positions of all markers are described in Table 2.
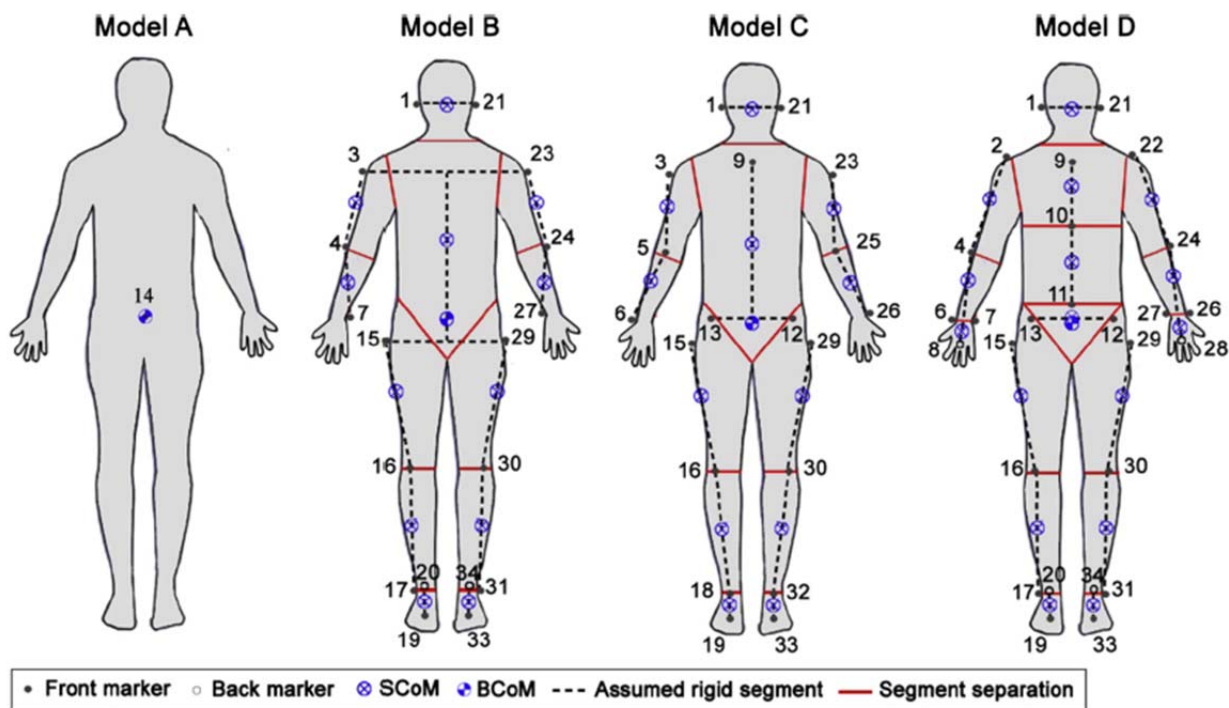

Figure 3: Frontal view of marker locations, body segments, SCoMs and BCoM for four models.

Model A consists of the sacral marker only (No. 14 in Fig. 3). This model was selected to test the hypothesis that one marker, which lies in the proximity of BCoM, can be used to determine the force [28]. Model B comprises of 18 markers to replicate the marker arrangement from a recent study of the walking force [19]. The movement of the trunk in this model is not directly monitored. Instead, it is determined by interpolation from the shoulder and the hip markers (Fig. 3). This approach might introduce a nonnegligible error in the calculation of the inertia

force of the trunk, and potentially a large error in the total force given that the trunk provides the largest contribution to the body mass (Table 1). Model C consists of 19 markers located on the frontal part of the body only. This setup, proposed by the authors, aims to minimise the number of cameras required for the experiments. The associated reduction in costs of experiments might be an important factor for future studies related to monitoring of test subjects outside the laboratory. To improve monitoring of the trunk (compared with Model B), Model C utilises three markers placed either directly on the trunk (No. 9 in Fig. 3) or in its vicinity (No. 12 and 13). A potential issue with this model is that placing markers exclusively on the frontal part of the body could result in the ankle (No. 18 and 32) and elbow markers (No. 5 and 25) not necessarily being attached to the bony landmarks. This issue might introduce the soft tissue artifact errors during measurements. Additional error could be introduced due to monitoring feet by utilising ankle and toe markers only, i.e. due to neglecting the heel contribution. To address the issues associated with Model C, the authors also propose Model D that includes a detailed instrumentation of the human body using 27 markers (Fig. 3). Apart from an improved instrumentation of feet in Model D, monitoring of the trunk is also improved by splitting it into three parts (i.e. upper, middle and lower trunk). The intention is to track movements of different parts of the trunk and investigate whether this approach leads to a better quality of the force measured. In addition, hand movement is also recorded in Model D.

Apart from the layouts of markers in the four models, Fig. 3 also shows individual body segments, the SCoMs and the BCoM in all models under investigation. The locations of SCoMs and BCoM are calculated using data from de Leva [23].

Table 2
Marker positions in the four marker models.

Body segment	Marker number	Anatomical position	Model
Head	1, 21	Cheek bone	B, C, D
Arms	2, 22	Bony prominence at the top of shoulder joint	D
	3, 23	Upper arm, at the same longitudinal elevation with shoulder joints	B, C
	4, 24	Bony prominence on the outside of the elbow joint	B, D
	5, 25	On biceps tendon at the location of elbow joint	C
	6, 26	Radial styloid process at wrist joint	C, D
	7, 27	Ulnar styloid process at wrist joint	B, D
	8, 28	Just below the middle knuckle on the hand	D
Trunk	9	Top of the breast bone	C, D
	10	Base of the breast bone	D
	11	On top of the navel fixed in position by using a wrap band	D
	12, 13	Anterior superior iliac spine	C, D
	14	Midpoint of the two posterior superior iliac spines	A
Legs	15, 29	Greater trochanter	B, C, D
	16, 30	On knee cap, at the elevation of knee joint centre	B, C, D
	17, 31	Lateral malleolus	B, D
	18, 32	On the extensor hallucis longus muscle, at the elevation of ankle joint centre	C
	19, 33	Tip of big toe	B, C, D
	20, 34	On the back of the foot, at the elevation of toe markers	B, D

2.3 Description of experiments

Ten male TSs with no history of gait issues volunteered to participate in the tests performed in the Gait Laboratory. The general characteristics of the TSs, in terms of the average ± one standard deviation, are: age 22.7 ± 2.7 years, height 177.5 ± 5.6 cm and mass 69.3 ± 7.7 kg. Test participants were requested to stay topless and to wear a pair of black tight running shorts so that most markers could be placed directly on the skin, minimising the risk of loose attachment. The markers were glued to the TS's body using double-sided tape. Before starting experiments, the TSs were instructed to quietly stand on the force plate for 30 s. The average of the vertical component of the recorded force plate signal was then divided by the acceleration of gravity to determine the body mass.

Evaluation of the accuracy of the marker models can be performed by comparing the indirectly recorded force against the benchmark force measured directly by the force plate. Comparison of the data acquired in the walking posture poses a challenge: the single force plate setup records the force generated by a single foot only, while the MCS records the total force. To make the comparison possible, a decision was made to ask TSs to perform an on-the-spot activity so that both facilities can record the total force (over a prolonged time period). Among candidate on-the-spot activities, such as jumping, bouncing and stamping, the stamping was chosen due to movement of limbs during this activity being most similar to that in walking. Since human kinematics during stamping is similar but not the same as that during walking, the results from the evaluation of the four models were used to identify a single, most promising, marker model, and then to evaluate it in a more relevant (and more demanding) experimental setup related to walking over a laboratory bridge.

Each TS was required to stamp on the force plate, with the assistance of a metronome, at eleven frequencies between 1.5 Hz and 2.5 Hz. The stamping frequencies and their order of execution were 1.7, 2.0, 1.8, 2.3, 1.6, 2.1, 2.5, 1.9, 2.4, 1.5 and 2.2 Hz. The pseudorandom order was employed to avoid possible psychological bias associated with using exclusively either increasing or decreasing pacing rate order. Each TS completed three consecutive trials at any particular frequency before proceeding to the next frequency.

Recording in a trial started when the TS declared himself comfortable with following the metronome beat. The duration of each recording was 60 s. After three trials at a single frequency, there was a short break of 30 s. During this break, the attachment of the markers to the body was checked. If a loose marker was detected, the previous three trials were repeated. In addition, rare trials in which TSs accidentally stepped out of the force plate were also repeated. Overall, each TS completed 33 trials that qualified for the analysis. Each test session lasted 1.5–2.5 h.

2.4 Evaluation of four marker models

Marker trajectories and force plate data were sampled at 200 Hz. To remove high-frequency noise (e.g. electrical noise in the optoelectronic system and soft tissue artifact) both the marker and the force plate data were filtered in MATLAB [29] using a fourth-order zero-phase-shift low-pass filter with the cut-off frequency of 10 Hz [27,30]. The displacement data were then differentiated twice to calculate the accelerations of the markers. The stamping force was then determined using Eq. (2).

Fig. 4a shows an example of a time-domain force signal directly measured using the force plate (solid line) and the corresponding signal calculated from the kinematic data recorded by the MCS using Model C (dashed line). Only the dynamic component of the stamping force F_D is presented in the figure. Fig. 4b represents the frequency content of the two signals in the vicinity of the fundamental harmonic. In this particular case the indirectly measured amplitude of the first harmonic underestimates the directly measured value by 12%.
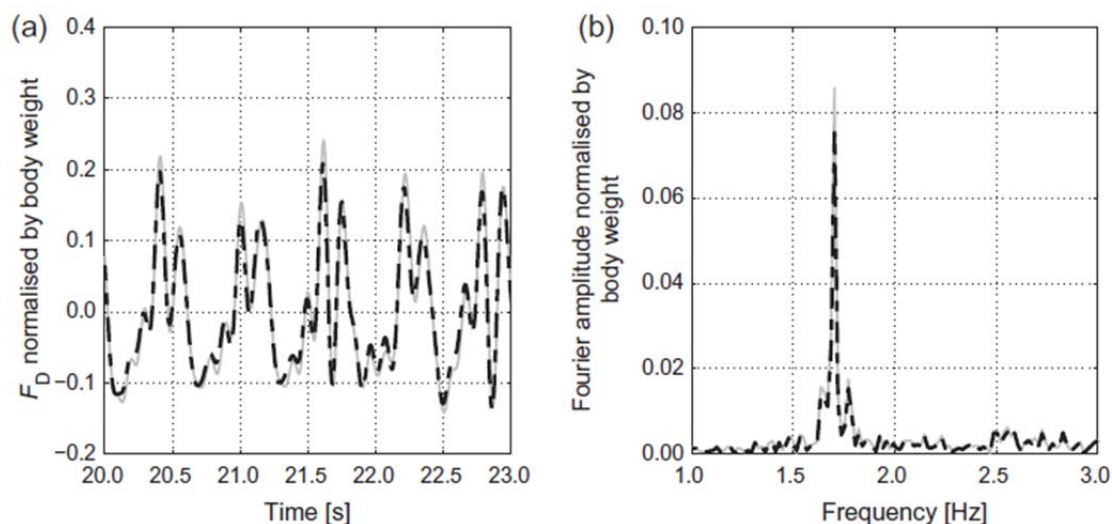

Figure 4: Directly measured force (solid line) and indirectly measured force (dashed line) in (a) time-domain and (b) frequency-domain.

To extract the first harmonic, the force signals were band-pass filtered using a fourth-order Butterworth filter and normalised by the test subject's weight. The filter bandwidth was set to

six standard deviations of the stamping frequency and centred at the average stamping rate. The peak-per-cycle amplitudes of the filtered signals were averaged to estimate directly and indirectly measured DLF_1. The percentage difference Δ_{DLF1} between the two sets of measurements:

$$\Delta_{DLF_1} = \frac{DLF_1^{MCS} - DLF_1^{Force\ plate}}{DLF_1^{Force\ plate}} 100\ (\%) \tag{3}$$

is shown in Fig. 5 in relation to individual TSs for all four models. Each data point in the figure represents the average difference over the three trials performed by a TS at a particular frequency. Model A underestimates the directly measured DLF_1 in all cases, with the absolute percentage difference being as high as 78%. Model B experiences a wide range of errors (from underestimating the force by 12% to overestimating it by about 38%). Given that Model B overestimates the force in 90% of cases, this model can be utilised for a conservative estimate of the dynamic force. For most accurate measurements of the stamping activity, however, Models C and D are recommended. These models result in the absolute percentage difference of up to 15% for 90% of TSs (i.e. all TSs but TS10). This finding suggests that a more detailed tracking of body segments employed in Model D (consisting of 27 markers) does not improve the measurement accuracy compared with Model C (consisting of 19 markers).

The results in Fig. 5 show that the measurement accuracy is influenced by the choice of the marker model and that Models C and D perform best. Since Model C utilises fewer markers, this model is selected for further evaluation in relation to the walking activity.
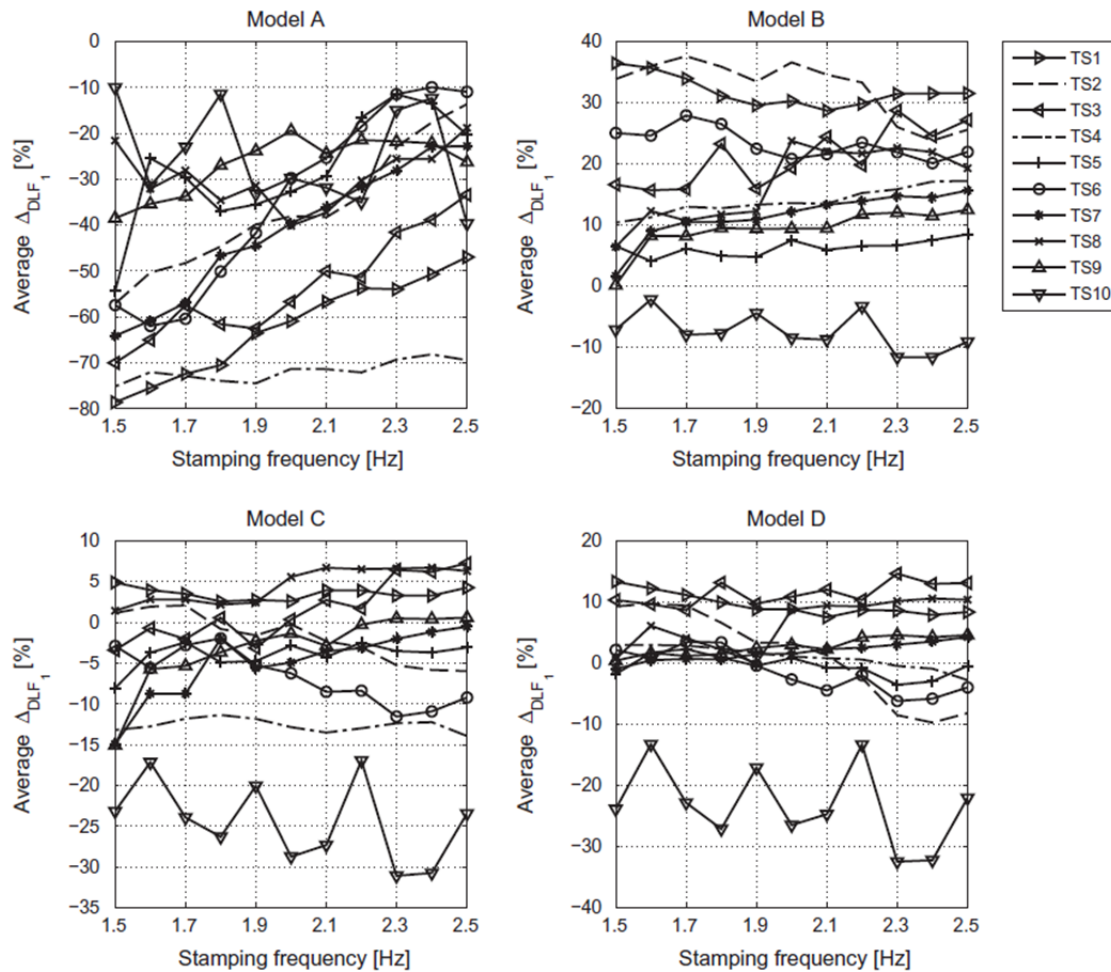
Figure 5: Percentage difference in DLF1 between indirectly and directly measured forces.

2.5 Evaluation of Model C while walking

To evaluate the suitability of Model C for measuring the walking-induced force, a subset of three test subjects were asked to walk on a treadmill device [31] placed on the Warwick Bridge (WB) situated in the Structures Laboratory at the University of Warwick. The steel–concrete composite bridge has a 2 m wide and 19.9 m long deck. The structure is simply supported, and the supports can be moved to alter the span length. In this study, two configurations of the bridge were utilised: the span length of 16.2 m (hereafter referred to as WB1) and the span length of 17.4 m (hereafter referred to as WB2). The natural frequency and the damping ratio of the fundamental mode of vibration were identified from free decay measurements and they were found to be amplitude dependent (Fig. 6). Using a controlled resonance build-up methodology developed by Brownjohn and Pavic [32], modal masses of the two structures

(including the treadmill) were found to be 7700 kg for WB1 and 8200 kg for WB2. More detailed information about the structural geometry and testing methodology is provided by Dang [33].
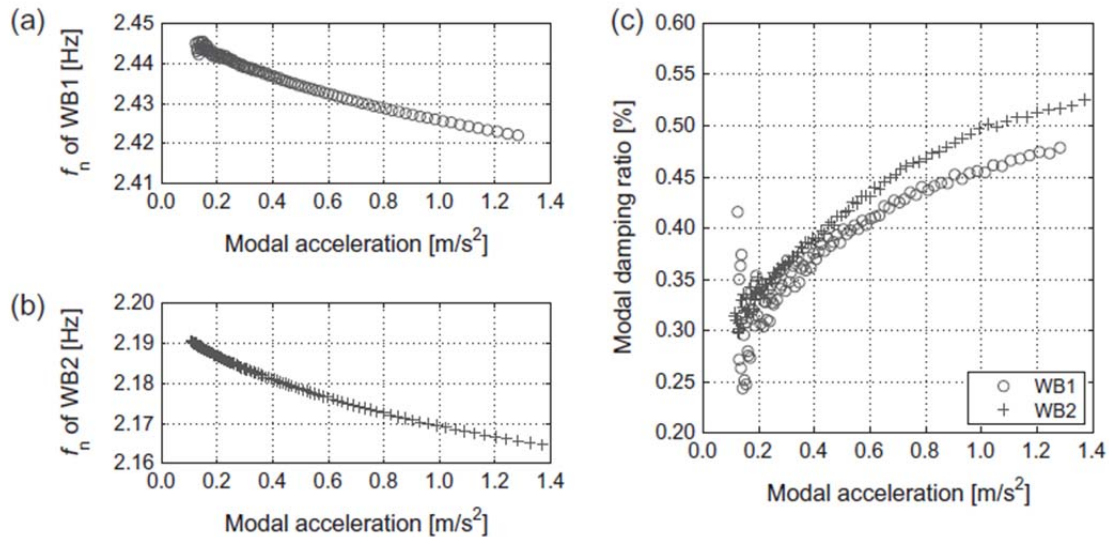

Figure 6: (a) Natural frequency of WB1, (b) natural frequency of WB2 and (c) damping ratio for the two bridge configurations as functions of vibration amplitude.

The treadmill was positioned at the midspan of the WB so that its longitudinal axis was aligned with the longitudinal axis of the bridge (Fig. 7a). Its belt accommodates speeds from 0.28 m/s to 5.00 m/s, with the speed resolution of 0.028 m/s. The treadmill walking area of 0.5 x 1.4 m (width x length) provides sufficient space for a single TS. Prior to the experiments, each TS had a 15-min warm-up and familiarisation with walking on the treadmill exercise at a number of personally selected walking speeds within the range 0.8–2.1 m/s, typical of normal walking [11]. Walking on the treadmill is known to differ from the over-ground walking due to the effects such as the imposed constant speed and stationary visual reference [34]. Van de Putte et al. [35] found that a 10 min warm-up on treadmill is required for differences between overground and treadmill walking to become negligible, leading to adopting the 15-min long practice on the treadmill in the experimental study presented in this paper.

After the calibration of the measurement system, the TS was instrumented using 19 markers (Model C) and his kinematics was monitored using three Vicon cameras attached to a frame built around the bridge (Fig. 7a). The global coordinate system for data capture was chosen to be aligned with the treadmill geometry, as shown in Fig. 7a. Data capturing started 30 s after the speed selection allowing the treadmill to reach the target speed and the TS to achieve a stable walking gait. A minimum of 450 steps were recorded in every trial to acquire statistically significant data [36].
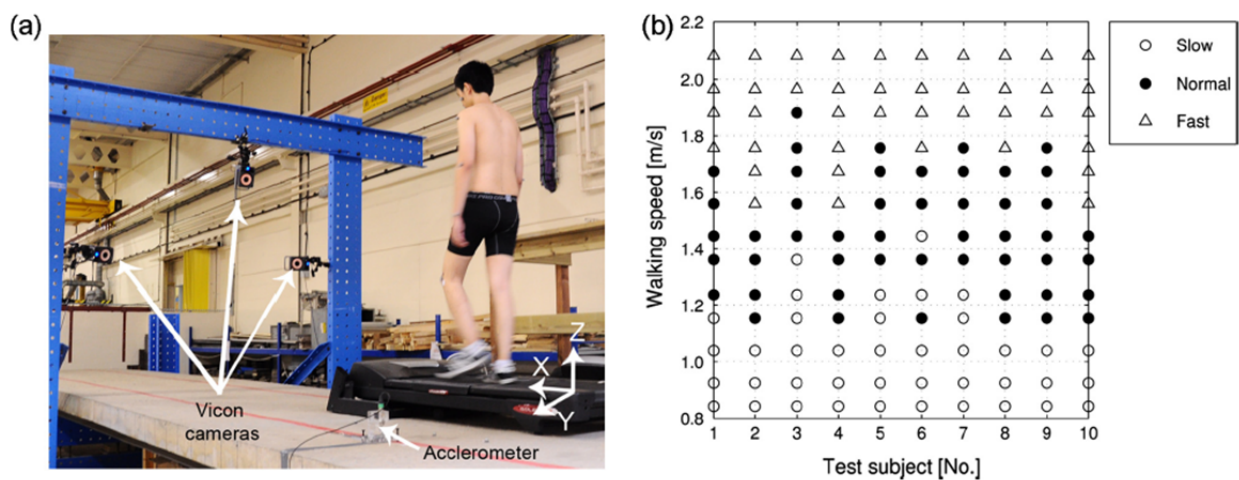

Figure 7: (a) Experimental setup on the Warwick Bridge. (b) Human perception of treadmill speed. Triangles, solid circles and empty circles represent fast, normal and slow classification of the walking speed, respectively.

Each TS was asked to walk at 5–7 different speeds (between 0.84 m/s and 2.08 m/s) on the two bridge configurations, with a three minute break between two consecutive trials. The three TSs performed 40 trials in total. In addition to measuring the TS's kinematics, the bridge oscillations were monitored using a QA750 Honeywell accelerometer (having a nominal sensitivity of 1300 mV/g). The accelerometer signal was logged alongside the Vicon data using the MX Giganet data logger [25].

The force induced by the pedestrian was determined in the same way as in Section 2.4 and then applied to a single-degree-of-freedom model of the bridge (having known natural frequency, damping ratio and modal mass) to calculate a modal acceleration response. The

initial conditions for the bridge were also known: the displacement was recorded by monitoring a marker placed at the midspan, while the velocity was obtained by differentiating the displacement signal. To account for the nonlinearities in the natural frequency and damping ratio, the modal parameters were updated on a cycle-by-cycle basis utilising the empirical values shown in Fig. 6 [33]. To extract the modal response in the fundamental mode of vibration, the simulated and the measured responses were band-pass filtered using a fourth-order Butterworth filter, with cut-off frequencies at 1 Hz and 3 Hz. The percentage difference in the average peak per cycle acceleration value for the two responses (relative to the measured value) was found to be within ±15% in as many as 78% of the trials, while it was within ±20% in 92% of the trials [33].

The increase in the response error compared with the ±15% error in 90% of trials related to the stamping activity is either due to increased measurement error in the walking-induced force (compared with the stamping activity), or the contribution of the (inherent) measurement error in the estimated modal properties of the bridge, or a combination of the two. A conservative conclusion is that the absolute value of the error in the measured walking force is, at worst, 20% in 92% of trials. Thus Model C can be used for applications that do not require a higher level of accuracy, for example for detecting change in force level on lively surfaces on which a force drop, as large as 75%, can occur [33]. Having quantified the error, Model C was adopted for experiments in the next section.

3   Experimental setup for monitoring walking locomotion

Ten young and healthy male TSs volunteered to participate in the main experimental programme for characterising walking locomotion in the Gait Laboratory. The characteristics of this sample, in terms of the average ± one standard deviation, are: age 25.0 ± 2.9 years, height 176.8 ± 5.4 cm and mass 72.4 ± 9.6 kg.

To monitor the walking gait over multiple steps in the confined laboratory space, the treadmill used for the experiments on the WB was placed in the centre of the capture room. In addition to the 19 markers required for the measurement of the force, the TSs were instrumented with two additional markers at the heels (No. 20 and 34 in Fig. 3) to allow for identification of the heel-strike events (required for quantifying a number of locomotion parameters). The following parameters were measured simultaneously: the pacing frequency, step length, step width, attack angle, end-of-step angle, trunk rotation and DLF_1.

The TSs were prepared for experiments on the treadmill in the same way as explained in the previous section. Within one test session lasting about two hours, a TS completed 13 trials at walking speeds ranging from 0.8 m/s to 2.1 m/s. The imposed belt speeds followed this pseudo-random order: 1.15, 1.56, 1.36, 1.88, 1.67, 2.08, 1.76, 1.04, 1.24, 0.84, 0.93, 1.97 and 1.45 m/s. In total, 130 trials, each consisting of about 450 steps, were recorded.

At the end of each trial, the TS was asked to subjectively categorise the speed as slow, normal or fast. These answers are shown in Fig. 7b as empty circles, filled circles and triangles, respectively. Apart from TS6, all other TSs were consistent in classification of the walking speed, i.e. they did not assess a speed as, say, fast even though some higher speeds were classified as normal or slow. Although this classification might have been biased due to TSs being asked to set up a particular speed on the control board of the treadmill before a trial, it still provides a useful indication of the normal walking speed range for each individual. It is worth mentioning that two successive trials were about five minutes apart, so the TSs were unlikely to remember the previously used speed and the reported classification of it, as confirmed by TSs at the end of their participation. All TSs used all three categories in their answers, suggesting that the tests succeeded in making the TSs walk both within and outside their comfortable (i.e. normal) speed range.

4   Statistical characterisation of walking parameters

This section provides a statistical description of both inter- and intra-subject variability of the monitored walking locomotion parameters. First the pacing rate, which is the key temporal parameter, is presented, followed by results for two spatial parameters (step length and step width). Angular positions of legs and trunk are then investigated, followed by the analysis of DLF_1. All the measured parameters are expressed as functions of the walking (i.e. treadmill belt) speed that is considered as an independent variable in this study.

4.1   Pacing rate

The pacing rate f_p is calculated as the reciprocal value of the duration of a walking step. The step duration is measured as the time elapsed from the heel-strike event of one foot to the heelstrike event of the other foot. To detect these events, a method proposed by Zeni et al. [37] is used. The method is based on the observation that, when walking on a treadmill, the X coordinate (Fig. 7a) of the heel marker changes from moving forward to moving backward at the heel-strike event (solid lines in Fig. 8a). This corresponds to change in the X component of the velocity vector (dashed lines in Fig. 8a) from a positive to a negative value. The detected zero crossings in the velocity signal (circles in Fig. 8a) are then used to calculate period T_i of each step leading to the calculation of the step frequency on a step-by-step basis.

An example of the pacing rate induced by left and right feet of a TS walking at the speed of 1 m/s is shown in Fig. 8b. It can be seen that there is some variation in the pacing rate around the mean value of 1.52 Hz (CoV = 2.8% in this example). The average pacing rate is shown as dashed line in the figure, while the average ± one standard deviation boundaries are given as dash-dotted lines. Fig. 8c shows that the probability density function (PDF) for this set of experimental data (dotted line) approximately follows a normal distribution (solid line). The Kolmogorov–Smirnov test for goodness-of-fit [38] was used to test the hypothesis that the data belong to a normal distribution. For the significance level of 5%, the hypothesis was rejected in 10% of trials only. An example of a trial in which the hypothesis was rejected is that shown in

Fig. 8c, while an example of a better agreement between the two distributions (related to a trial in which the hypothesis was not rejected) is shown in Fig. 8d. Therefore the step-by-step variations in the pacing rate can be modelled as normally distributed.

The average pacing rate and the corresponding CoV are calculated for each trial. These parameters are shown in Fig. 9 for individual TSs and walking speeds. Best least square second-order polynomial fit of the mean value (solid lines) and one standard deviation boundaries (dashed lines) across the TS population are also shown in the same figure. Subscripts ''u'' and ''l'' refer to the upper and lower boundaries of the standard deviation band. It can be seen that the average pacing rate increases with an increase in the walking speed.
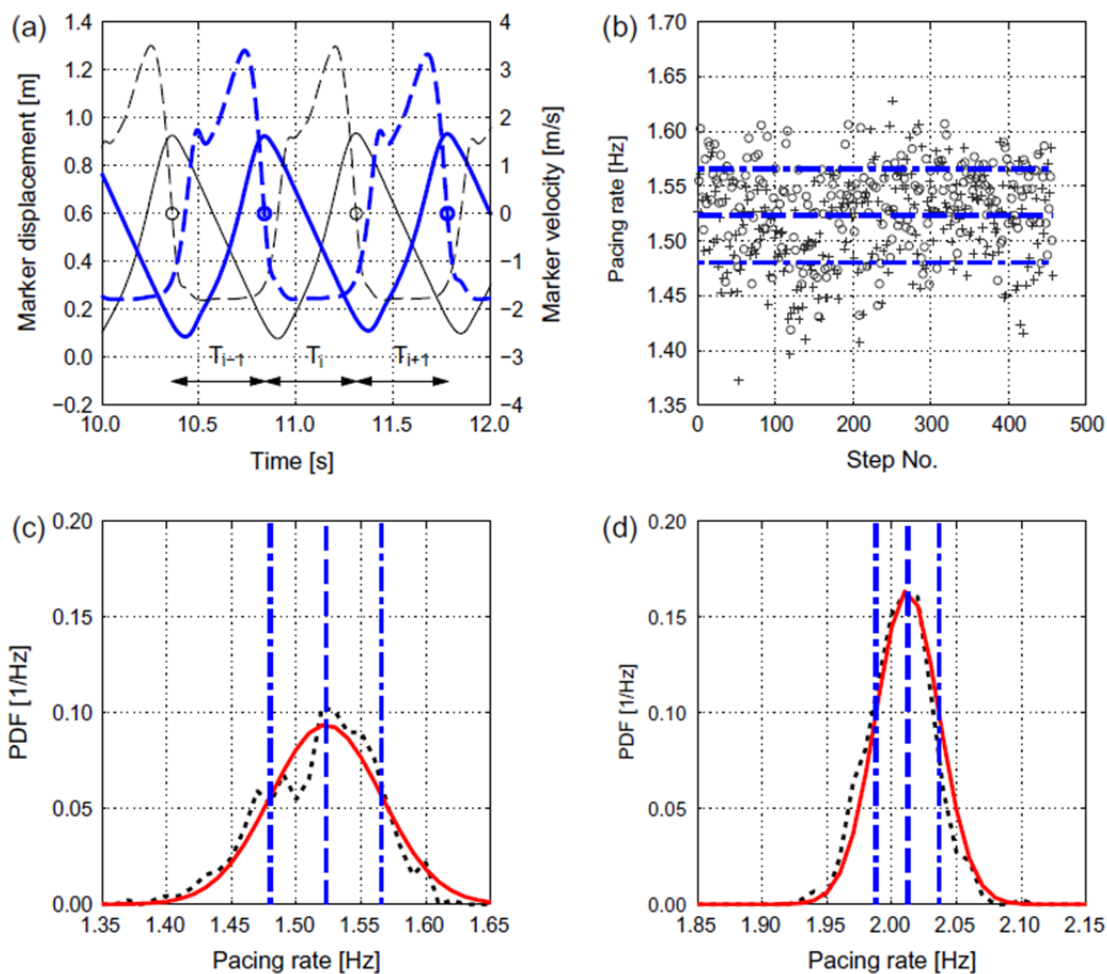

Figure 8: (a) X-component of displacement (solid lines) and velocity (dashed lines) of the heel markers. Thick lines: left foot, thin lines: right foot. (b) Pacing rate determined on a step-by-step basis. Circles: left foot, crosses: right foot. (c) and (d) PDFs of the measured pacing rate (dotted lines) and the corresponding normal distribution model (solid lines). Dashed lines: mean value, dash-dotted lines: mean ± one standard deviation.
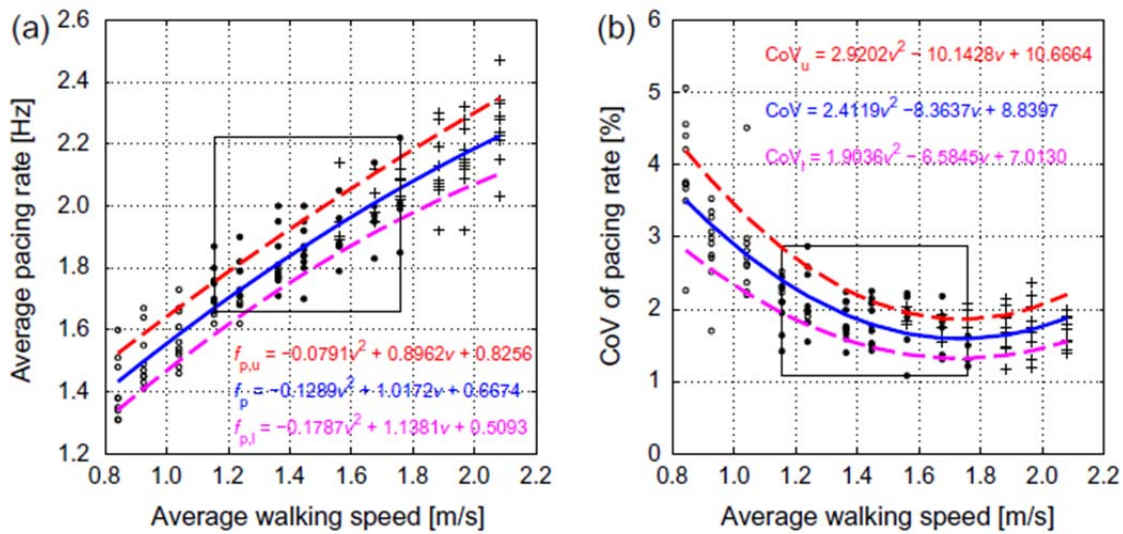
Figure 9: (a) Average and (b) CoV of pacing rate as functions of walking speed. Solid lines: best fits of mean values, dashed lines: best fits of one standard deviation bands. Empty circles: slow speed, filled circles: normal speed, crosses: fast speed. Rectangular areas: normal speed trials.

Fig. 9 also conveys the information about the TS's perception of the walking speed. Empty circles represent slow speed, filled circles are related to normal speed, while crosses represent fast speed. The rectangular area in the figure is a subset that includes all trials in which the speed was classified as normal (1.15–1.76 m/s). The average pacing rate over the normal speed range is between 1.66 Hz and 2.22 Hz, while the CoV over the same range is between 1.1% and 2.9%. The CoV is at its minimum when the TSs walked at the speeds within the normal-to-fast walking boundary.

Statistical characterisation of the pacing rate shown in Fig. 9 is used as a template for presentation of the data related to other walking locomotion parameters in the remainder of this section.

4.2 Spatial parameters

Step length d is the longitudinal distance (X direction in Figs. 7a and 10) that a pedestrian travels between two successive heelstrikes. A way to measure the step length is to determine

the distance between the heel markers on the two feet at the time of a heel-strike event of the leading leg (Fig. 10). This method induces an underestimation of the step length since the heel of the trailing leg is airborne at the heel-strike event of the leading leg. However, the error is small (about 2% of the step length) and it is neglected in this study.
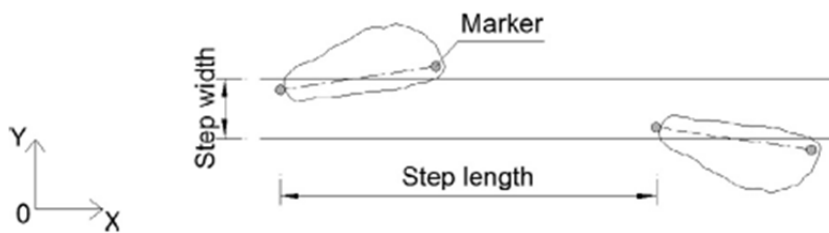

Figure 10: Step length and step width.

The step width is the lateral distance (Y direction in Figs. 7a and 10) between the centres of the two feet [17], where the centre of each foot is approximated as the midpoint between the toe and the heel markers (Fig. 10). The step width is also determined at the heel-strike event of the leading leg.

As in the case of the pacing rate, the empirical PDFs of the step length and step width are found to follow a normal distribution (the hypothesis of normal distribution is rejected in 10% and 1% of trials, respectively). The average step length and the corresponding CoV are shown in Fig. 11a and b, respectively, while these parameters for the step width are presented in Fig. 11c and d.

The average step length increases with an increase in the walking speed, while the CoV is at minimum at the walking speeds around the boundary between normal and fast walking. The average step length for normal speed lies in the range of 0.56–0.84 m. The average step width ranges from 60 mm to 143 mm on the normal speed range, and is similar elsewhere. The CoV of the step width also seems to be almost independent from the walking speed. The CoV for

the step width (13.4–39.2% on normal speed range) is significantly larger than that for the step
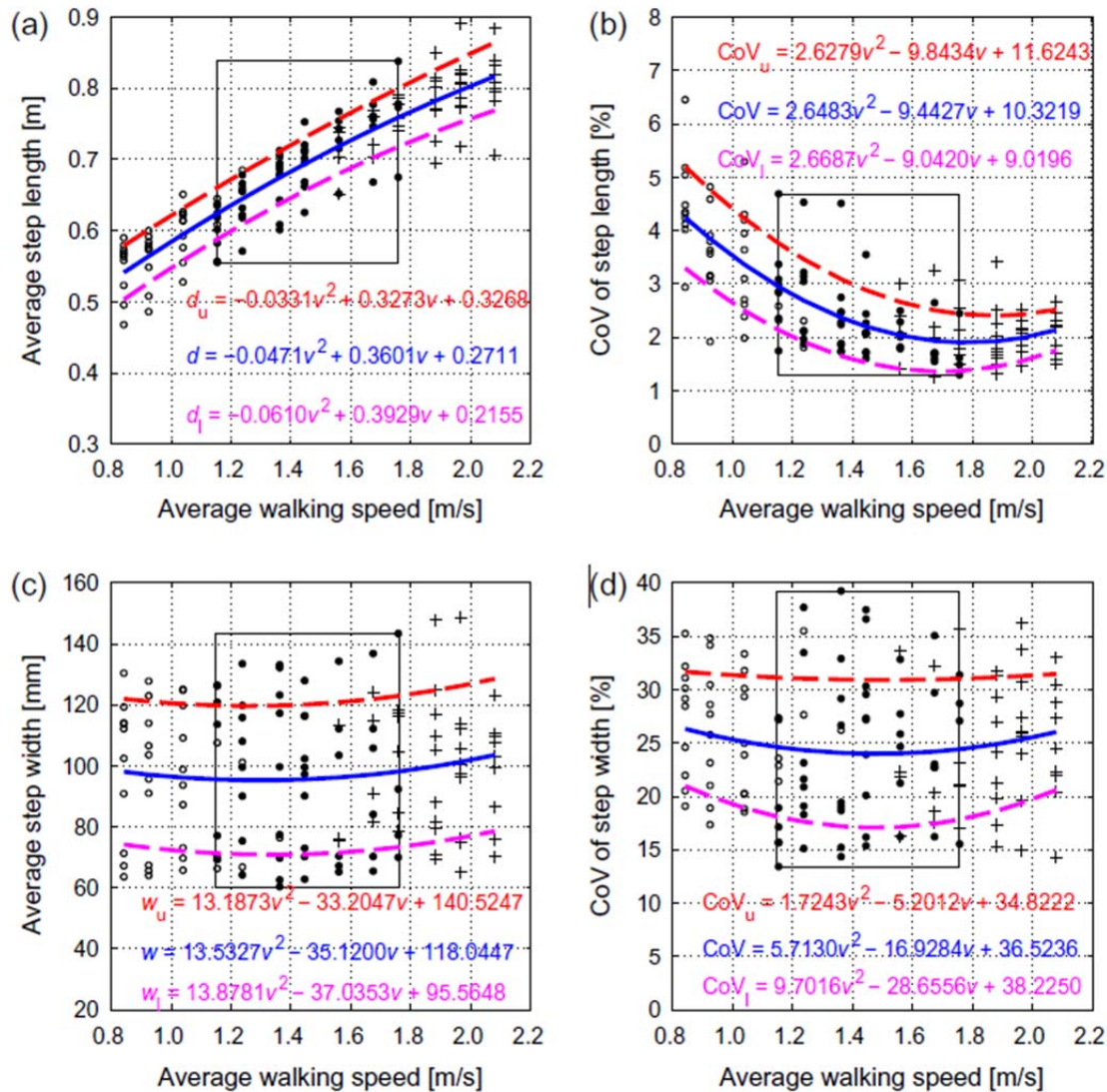
length (1.3– 4.7%).

Figure 11: (a) Average and (b) CoV of step length as functions of walking speed. (c) Average and (d) CoV of step width as functions of walking speed. Solid lines: best fits of mean values, dashed lines: best fits of one standard deviation bands. Empty circles: slow speed, filled circles: normal speed, crosses: fast speed. Rectangular areas: normal speed trials.

4.3 Angular parameters

This section describes three angular parameters: attack angle θ_0, end-of-step angle θ_e and

trunk orientation θ_{tr} (Fig. 12).

The attack angle is calculated at the heel strike events of the leading leg using measured coordinates of the ankle and BCoM (calculated using Model C) in the coordinate system shown in Fig. 7a:

$$\theta_0 = \tan^{-1} \frac{z_{BCoM} - z_{ankle}}{x_{ankle} - x_{BCoM}} \tag{4}$$

while the end-of-step angle is defined as:

$$\theta_e = 180° - \tan^{-1} \frac{z_{BCoM} - z_{toe}}{x_{BCoM} - x_{toe}} \tag{5}$$

Results of the Kolmogorov–Smirnov goodness-of-fit test show that, at 5% significance level, the hypothesis that θ_0 and θ_e follow the normal distribution is rejected in 3% of trials in both cases. The average value and the CoV for the attack angle are shown in Fig. 13a and b, respectively, while the same parameters for the end-of-step angle are presented in Fig. 13c and d. For the normal walking speed range, θ_0 = 69.1–77.3° (CoV = 0.6–2.1%) and θ_e = 107.8–119.2° (CoV = 0.3–1.0%).

With an increase in the walking speed, the attack angle reduces while the end-of-step angle increases due to increase in the step length (Fig. 11a). The best fit function for the sum of these two angular parameters with respect to the speed v (m/s) is:

$$\theta_0 + \theta_e = 5.0v + 180.1 \tag{6}$$

In all trials this sum is greater than 180° that is, due to geometry constraints i.e. lack of foot modelling, assumed in simple bipedal model [9]. This finding can be utilised in the development and validation of more advanced bipedal models (e.g. [10]).

The trunk is the biggest body segment, making around 72% of the mass of the upper body [23]. The trunk angle (Fig. 12b) in this study is defined with respect to a line connecting the sternum

marker and the midpoint of markers No. 12 and 13 in Fig. 3. These two points are referred to as the top trunk and the bottom trunk points, respectively. The angle htr is calculated as:

$$\theta_{tr} = 90° + \tan^{-1} \frac{x_{top\ trunk} - x_{bottom\ trunk}}{z_{top\ trunk} - z_{bottom\ trunk}} \tag{7}$$

The distribution of θ_{tr} calculated at the heel-strike events is found to follow a normal distribution (the hypothesis of normal distribution is rejected in 7% of trials). Fig. 13e shows that the trunk is relatively vertical for slow walking, i.e. the angle is close to 90° in these cases. As the speed increases, the angle increases indicating that TSs tend to lean forward at faster speeds. At normal walking speeds, the trunk angle ranges from 89.2° to 102.3°, while the CoV lies in the range of 0.6–1.3% (Fig. 13f).

From the continuous measurement of the trunk angle, its maximum variation within each individual step is also calculated. This value ranges between 1.6° and 3.5° when walking at normal speeds, confirming Winter's observation that the trunk rotation is small within any particular step [16].
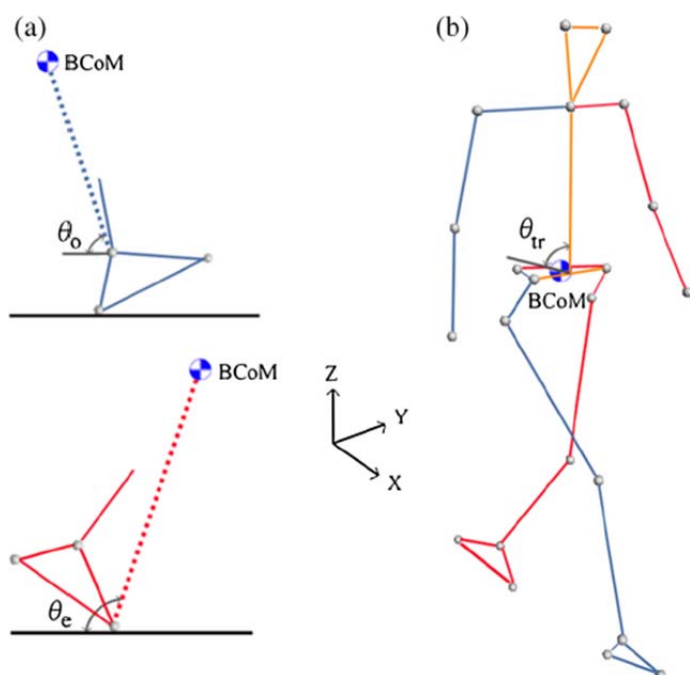

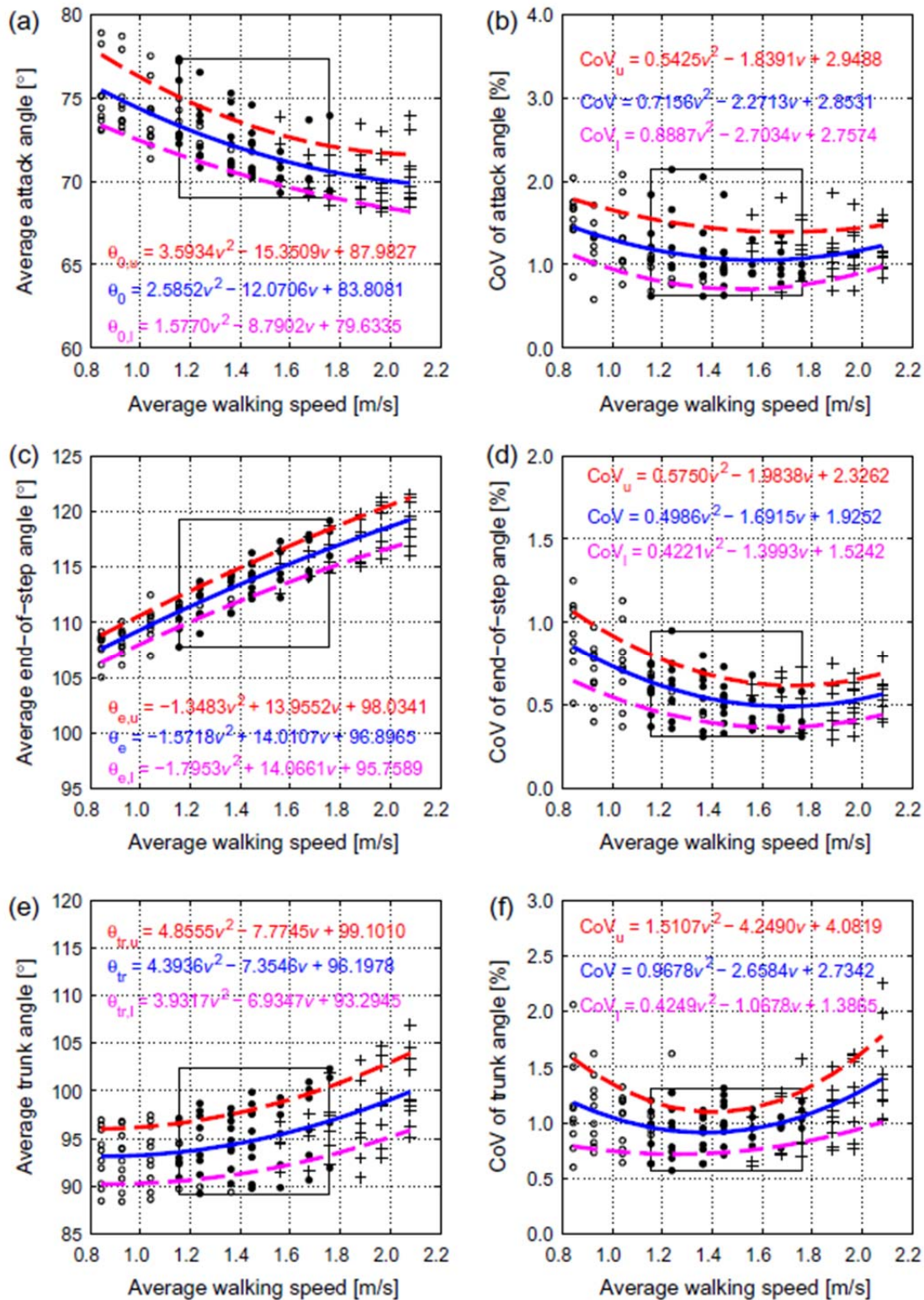Figure 12: (a) Angle of attack and end-of-step angle. (b) Trunk orientation.

Figure 13: (a) Average and (b) CoV of angle of attack as functions of walking speed. (c) Average and (d) CoV of end-of-step angle as functions of walking speed. (e) Average and (f) CoV of the trunk angle as functions of walking speed. Solid lines: best fits of mean values, dashed lines: best fits of one standard deviation bands. Empty circles: slow speed, filled circles: normal speed, crosses: fast speed. Rectangular areas: normal speed trials.

4.4 Dynamic loading factor

To determine DLF_1 on a step-by-step basis, indirectly obtained force signal was band-pass filtered using a fourth-order Butterworth filter. Given that the pacing rate was found to follow a normal distribution in Section 4.1, the filter bandwidth was set to include frequency lines within ± three standard deviations of the mean pacing rate. A time history of the narrow-band (i.e. filtered) force normalised by the body weight is shown in Fig. 14a, while the spectrum of the measured force and the frequency bandwidth used for filtering are shown in Fig. 14b. At 5% significance level, the Kolmogorov–Smirnov test suggests that DLF_1 follows the normal distribution in 62% of the trials only. DLF_1 deviates from the normal distribution more than the other parameters, possibly due to differences in the individual forces generated by the ''strong'' and ''weak'' leg [4]. The individual effects of the two feet could not be investigated using the MCS, and they should be subjected to further research.
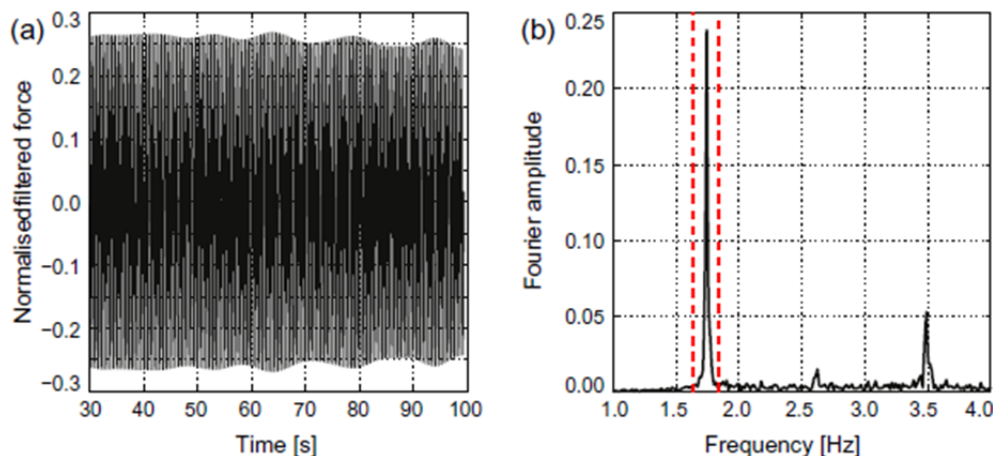

Figure 14: (a) Time-domain of the narrow-band force component around the first harmonic. (b) Fourier spectrum of the force (normalised to body weight). Dashed lines represent filter bandwidth.

The average value of DLF_1 increases with an increase in the walking speed (Fig. 15a), while the CoV is lowest when the walking speed is close to the boundary between normal and fast walking (Fig. 15b). For normal speed DLF_1 = 0.11–0.48 while CoV = 1.5–8.3%. DLF_1 and CoV are expressed as functions of the average pacing rate in Fig. 15c and d. Best fit functions for the average DLF_1 in this study (solid line) are compared with a study involving 40 TSs reported by

Kerr [14] (dashed line) and a three-TS study by Brownjohn et al. [2] (dash-dotted line). The results are consistent in reflecting that the DLF_1 increases with an increase in the pacing rate. However, the average DLF_1 in this study is consistently lower than that in the study by Kerr up to the pacing rate of 2.2 Hz (with differences being more pronounced at slower pacing rates) and consistently larger than the values reported in [2] for all but extremely slow walking speeds. These differences are a natural consequence of variations associated with different populations of test participants.
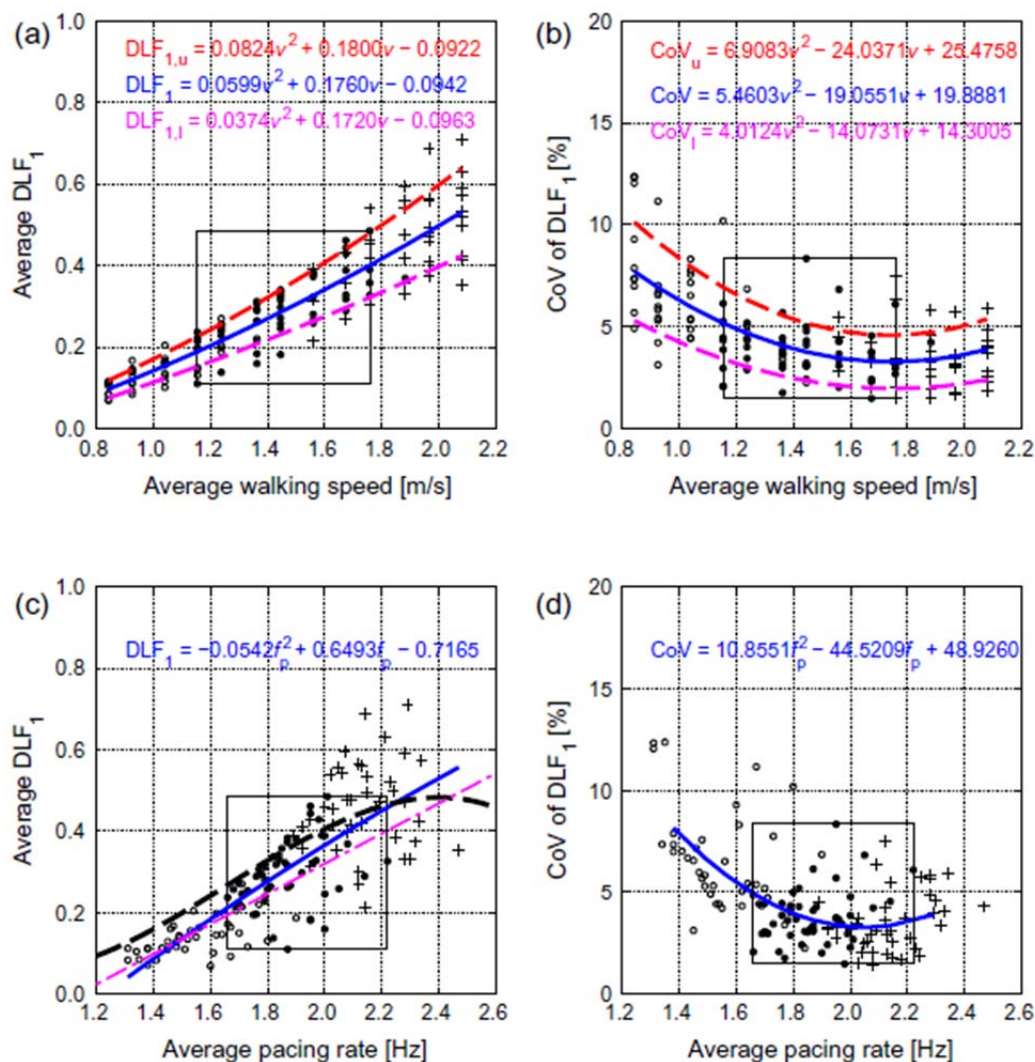

Figure 15: (a) Average and (b) CoV of DLF_1 as functions of walking speed. Solid lines: best fits of mean values, dashed lines: best fits of one standard deviation bands. (c) Average and (d) CoV of DLF_1 as functions of pacing rate. Solid lines: best fit functions of the mean values. Dashed and dash-dotted lines in (c) represent functions reported in [14] and [2], respectively. (a)–(d) Empty circles: slow speed, filled circles: normal speed, crosses: fast speed. Rectangular areas: normal speed trials.

5   Discussion and conclusions

The motion capture system Vicon in the Gait Laboratory at the University of Warwick has been utilised in this study for simultaneous monitoring of seven walking locomotion parameters, including an indirectly measured dynamic force. Although the use of MCSs in civil engineering research is growing, guidance related to the choice of the marker layout for force measurement is not readily available, motivating a study into four candidate models (consisting of 1–27 markers) in this paper. Due to limitations in the measurement system, their accuracy was evaluated only in relation to the stamping activity. It was found that two marker models (C and D), proposed by the authors, provide best accuracy, with measurement error in DLF_1 being up to 15% in 90% of trials. The precise description of the geometry of each model required for their use by independent researchers has been provided. Model C has advantages in that it utilises fewer markers, and that all markers are positioned on the frontal part of the body, allowing a reduced number of cameras to be used. Both of these advantages lead to the reduced cost of the testing and they are expected to prove extremely beneficial when performing measurements outside the laboratory. The performance of Model C was then tested in relation to the walking activity. The measurement error was found to be up to 20% in more than 90% of trials. As a result, Model C is recommended for force measurements for which the 20% accuracy is considered acceptable, for example when quantifying pedestrian-structure interaction on lively structures (on which a substantial drop in the forcing amplitude has been observed in the past [33]). Despite establishing potential of using Model C for this specific application, further research should be directed towards improvement of the measurement accuracy when utilising the MCSs.

After choosing the marker layout, ten test subjects walking on a treadmill were monitored using the Vicon system. Seven walking locomotion parameters were measured: the pacing frequency, step length, step width, attack angle, end-of-step angle, trunk rotation and DLF_1. All parameters were studied in relation to 13 walking speeds (ranging from 0.8 m/s to 2.1 m/s).

Within the investigated population, the walking speed subjectively perceived as ''normal'' was found to be in the range of 1.15–1.76 m/s. The ranges of numerical values for other parameters recorded when walking at normal speeds were found to be: 1.66–2.22 Hz for the pacing frequency, 0.56–0.84 m for the step length, 60–143 mm for the step width, 69.1–77.3° for the attack angle, 107.8–119.2° for the end-of-step angle, 89.2–102.3° for the trunk angle, and 0.11–0.48 for the DLF_1. The CoV over normal speed range was less than 5% for most parameters. The only exceptions were the DLF_1 (CoV = 1.5–8.3%) and a large variation for the step width (CoV = 13.4–39.2%). It is interesting to note that the CoV for all parameters, apart from the step width and the trunk angle, tended to reach minimum value at walking speeds at the boundary between normal and fast walking. This observation indicates that test subjects achieved the most consistent (i.e. least variable) walking pattern at this boundary.

It was shown in this paper that modelling intra-subject variations in all parameters using normal distribution is justified. The only exception is DLF_1 which should be further investigated to determine a better distribution model. In addition, further studies should include a larger sample of test subjects to allow for testing of mutual dependence of parameters across the pedestrian population.

The results presented in this paper provide a particularly detailed characterisation of the intra-subject variability in the walking parameters. These results can be used for calibration of bipedal class of pedestrian models for walking over rigid ground, in particular to test their capability of reproducing the established correlation with the walking speed and observed step-by-step variability.

Acknowledgements

References

[1] BSI Steel. Concrete and composite bridges—Part 2: specification for loads; appendix C: vibration serviceability requirements for foot and cycle track bridges, BS 5400. London, UK: British Standards Association; 1978.

[2] Brownjohn, J. M. W., Fok, P., Roche, M., and Omenzetter, P. (2004) Long span steel pedestrian bridge at Singapore Changi Airport—Part 2: Crowd loading tests and vibration mitigation measures." Structural Engineer, 82 (16), 28–34.

[3] Sétra (2006) Footbridges, assessment of vibrational behaviour of footbridges under pedestrian loading, technical guide, Service d'Etudes Techniques des Routes et Autoroutes, Paris.

[4] Živanović, S., Pavic, A. and Reynolds, P. (2007) Probability based prediction of multi-mode vibration response to walking excitation. Engineering Structures, 29 (6), 942-954.

[5] Racic, V. and Brownjohn, J. M. W. (2011) Stochastic model of near-periodic vertical loads due to humans walking. Advanced Engineering Informatics, 25 (2), 259-275.

[6] Piccardo G. and Tubino, F. (2012) Equivalent spectral model and maximum dynamic response for the serviceability analysis of footbridges. Engineering Structures, 40, 445–456.

[7] Caprani, C. C. (2014) Application of the pseudo-excitation method to assessment of walking variability on footbridge vibration. Computers and Structures, 132, 43-54.

[8] Ingólfsson, E. T. and Georgakis, C. T (2011) A stochastic load model for pedestrian-induced lateral forces on footbridges. Engineering Structures, 33 (12), 3454-3470.

[9] Bocian, M., Macdonald, J. H. G. and Burn, J. F. (2013) Biomechanically-inspired modeling of pedestrian-induced vertical self-excited forces. Journal of Bridge Engineering, 18 (12), 1336–1346.

[10] Qin, J. W, Law, S. S, Yang, Q. S. and Yang, N. (2013) Pedestrian-bridge dynamic interaction, including human participation. Journal of Sound and Vibration, 332 (4), 1107–1124.

[11] Živanović, S. (2012) Benchmark footbridge for vibration serviceability assessment under vertical component of pedestrian load. Journal of Structural Engineering, 138 (10), 1193-1202.

[12] Owings, T.M. and Grabiner, M. D. (2004) Variability of step kinematics in young and older adults. Gait Posture, 20(1), 26–19.

[13] Pedersen, L., and Frier, C. (2010) Sensitivity of footbridge vibrations to stochastic walking parameters. Journal of Sound and Vibration, 329 (13), 2683–2701.

[14] Kerr SC. Human induced loading on staircases. PhD thesis, Department of Mechanical Engineering, University College London, UK; 1998.

[15] Geyer H. Simple models of legged locomotion based on compliant limb behaviour. PhD thesis, Faculty of Social and Behavioural Sciences, Friedrich-Schiller-Universität, Jena, Germany; 2005.

[16] Winter, D. A. (1995) Human balance and posture control during standing and walking. Gait & Posture, 3(4), 193–214.

[17] Bauby, C. E. and Kuo, A. D. (2000) Active control of lateral balance in human walking. Journal of Biomechanics, 33(11), 1433–1440.

[18] Yamasaki M, Sasaki T, Torii M. (1991) Sex difference in the pattern of lower limb movement during treadmill walking. European Journal of Applied Physiology and Occupational Physiology; 62(2), 99–103.

[19] Racic. V., Brownjohn, J. M. W. and Pavic, A. (2010) Reproduction and application of pedestrian forces from visual marker data. In: Proceedings of the IUTAM symposium on analysis and simulation of human motion. Leuven, 13–15 Sep.

[20] Racic, V., Brownjohn, J. M. W. and Pavic, A. (2010) Reproduction and application of human

bouncing and jumping forces from visual marker data. Journal of Sound and Vibration, 329(16), 3397–3416.

[21] Bobbert, M.F., Schamhardt, H.C. and Nigg, B. M. (1991) Calculation of vertical ground reaction force estimates during running from positional data. Journal of Biomechanics, 24(12), 1095–1105.

[22] Racic, V., Pavic, A. and Brownjohn, J. M. W. (2009) Experimental identification and analytical modelling of human walking forces: literature review. Journal of Sound and Vibration, 326 (1–2), 1–49.

[23] de Leva, P. (1996) Adjustments to Zatsiorsky-Seluyanov's segment inertia parameters. Journal of Biomechanics, 29 (9), 1223–1230.

[24] Vaughan, C.L., Davis, B.L. and O'Connor, J. C. (1999) Dynamics of human gait. 2nd ed. Kiboho Publishers.

[25] Oxford Metrics Group (2007) Vicon user manual, Oxford, UK.

[26] AMTI. Force plate manual – model OR6-7. Advanced Mechanical Technology Inc, Watertown, MA 02472, USA; 2007.

[27] Hasan, S. S., Robin, D. W., Szurkus, D. C., Ashmead, D. H., Peterson, S. W. and Shiavi, R. G. (1996) Simultaneous measurement of body center of pressure and center of gravity during upright stance. Part I: methods. Gait & Posture, 4 (1), 1–10.

[28] Gard, S.A., Miff, S. C. and Kuo, A. D. (2004) Comparison of kinematic and kinetic methods for computing the vertical motion of the body center of mass during walking. Human Movement Science, 22(6), 597–610.

[29] Mathworks (2011) MATLAB version 7.13.0.564. Natick, Massachusetts, USA.

[30] Winte, D. A. (2005) Biomechanics and motor control of human movement. 3rd ed. John Wiley & Sons Inc.

[31] Fuel Fitness (2013) Treadmill user manual – model F63. Fuel Fitness Co., Ltd. Stoke-On-Trent, UK.

[32] Brownjohn, J. M. W. and Pavic, A. (2007) Experimental methods for estimating modal mass in footbridges using human-induced dynamic excitation. Engineering Structures, 29(11), 2833–2843.

[33] Dang, H. V. (2014) Experimental and numerical modelling of walking locomotion on vertically vibrating low-frequency structures. PhD thesis, School of Engineering, University of Warwick, UK.

[34] Bocian, M. (2014) Determination of the self-excited forces on structures due to walking pedestrians using biologically-inspired approach. PhD thesis, Faculty of Engineering, University of Bristol, UK.

[35] Van de Putte, M., Hagemeister, N., St-Onge, N., Parent, G. and de Guise, J. A. (2006) Habituation to treadmill walking. Bio-Med Mater Eng, 16 (1), 43–52.

[36] Owings, T. M. and Grabiner M. D. (2003) Measuring step kinematic variability on an instrumented treadmill: how many steps are enough? Journal of Biomechanics, 36(8), 1215–1218.

[37] Zeni Jr, J. A., Richards, J. G. and Higginson, J. S. (2008) Two simple methods for determining gait events during treadmill and overground walking using kinematic data. Gait & Posture, 27(4), 710–714.

[38] Massey Jr, F. J. (1951) The Kolmogorov–Smirnov test for goodness of fit. Journal of the American Statistical Association, 46(253), 68–78.